Evaluation of a Physical Based Approach of Scattered Radiation Correction in Cone Beam CT for Non-Destructive Testing Applications

Jean RINKEL, CEA-LETI, Grenoble France
François ESTEVE, INSERM U647-RSRM, Grenoble France
Jean-Marc DINTEN, CEA-LETI, Grenoble France

Abstract Cone Beam Computerized Tomography (CBCT) enables three-dimensional imaging with isotropic resolution. X-ray scatter management is a challenging task for quantitative CBCT imaging : scattered radiation level is significantly high on cone beam systems compared to collimated fan beam systems. The effects of this scattered radiation are cupping artifacts, streaks, and quantification inaccuracies. At CEA-LETI, an original scatter management process without additional on-line acquisition has been developed, the API (Analytical transformation Plus Indexation based) method. The proposed method is composed of two steps: a scatter calibration is first performed through off-line acquisitions and is used to evaluate the level and a global shape of scattered radiation on on-line tomographic projections of the object. This global shape is adapted to the current acquisition with an analytical transformation issued from physical equations to evaluate the scattered radiation distribution on tomographic projections. This approach has been applied successfully in medical field. This paper presents in detail the API method and evaluates it in CBCT for Non-Destructive Testing (NDT). To evaluate API method, experimental radiographic projections of simple geometry objects were performed with a Thales Flaschscan flat panel detector and corrected from scatter by API method and by a beam stops method. Simulated projections of primary radiation were performed with the simulation software Sindbad, developed at CEA LETI. Reconstructions were then performed on experimental scatter corrected projections and on simulated projections. The API method provides results in good agreement with simulations, suppressing cupping artifact. The improvements due to the scatter correction by the API method have the same order of magnitude as those due to the correction by the beam stops method on experiments performed without antiscatter grid. The estimation of scatter is found to be more accurate with the API method than with the beam stops method on experiments performed with an antiscatter grid. API method improves NDT quantitatively and qualitatively without increasing on-line acquisition time.

Introduction

The effects of scattered radiation in X-rays tomography are cupping, streaks, CT number inaccuracies and increase of noise. Developing an X-rays scatter estimation technique for quantitative cone beam computed tomography (CBCT) remains a big challenge because the amount of scatter is much higher compared to fan beam systems: the scattered radiation is often higher than the primary whereas it represents generally less than 20 % of the primary in fan beam systems.

Methods of scatter correction based on an analytical prediction of scatter have been proposed [1]. Monte Carlo simulations have been used to predict the scattered radiation in CBCT [2]. The main drawback of the Monte Carlo based techniques is the high computing time needed to have simulations representative of physical processes. A method of object scattering correction is based on the use of radio opaque absorbers, or beam stops, placed in the beam to absorb all primary radiations [3]. Thus, scattered radiation images are calculated by interpolation and subtracted to acquisitions. The beam stops method of correction of scattered radiation has to be applied on every projection of the tomographic acquisition. The main drawback of this method is the significant increase in terms of acquisition time, at least twice the original acquisition time.

Anti scatter grids limit the amount of scatter reaching the detector, and reduce significantly scatter degradation [4]. Nevertheless a scatter correction is still required, because the residual signal portion of scatter can outweigh the primary. Furthermore, the main drawback of the grids is that a part of the primary radiation is absorbed by the grid.

This study aims to propose an original scatter management approach based on the estimation of spatial distribution of scatter in the detector plane and to evaluate it for Non Destructive Testing applications. In this method, scatter is calibrated off-line through measurements performed with lucite plates and no supplementary acquisitions of the examined object are required. The method is evaluated on two different configurations: first, tomographic acquisitions of a lucite phantom with two cylindrical holes are performed without anti scatter grid. Secondly, the method is evaluated on acquisitions of a phantom composed of water and comprising metallic inserts performed with an antiscatter grid. A beam stops approach is adapted to our experimental bench and the results obtained with the beam stops approach are compared with those obtained with the new method.

1. Scatter correction method

1.1 Introduction

In this part, an original processing of scatter which does not require on-line supplementary acquisitions is described. This method is inspired by an approach developed to correct X-rays scatter for Dual Energy X-rays absorptiometry [5] and has been applied successfully in medical field [6] [7]. It evaluates the level and the global shape of scattered radiation image from calibration acquisitions and adapts it to acquisitions. Therefore, weighting parameters are determined from acquired image by deriving the equations which describe first-order Compton interaction of the X-rays beam within the examined object. The presented approach has been extended to tomographic acquisitions: 3D information issued from a first reconstruction are used to evaluate the transposition coefficients more precisely. This approach is based on the

three following steps:

1. For each tomographic projection, a lucite equivalent scattered radiation map is selected, by comparison of the total measurement radiation value between calibration acquisitions and the examined tomographic projection.

2. Transposition coefficients between the scatter map of lucite and that of the examined object are computed. These coefficients are functions of the total measured radiation through lucite and through the examined object and of the 3D information obtained by a first tomographic reconstruction.

3. The scattered radiation maps obtained from the calibration data set are weighted by the transposition coefficients.

1.2 Scatter process modelization

The model of scatter assumes that the scattered radiation distribution in the detector plane $\phi_S(x, y)$ can be expressed as a function of the two-dimensional convolution of a scatter potential $P(x, y)$ with the point spread function of object scattering, $K_O(x, y)$:

$$\boxed{\phi_S(x, y) = A(x, y) \times (P(x, y) * K_O(x, y))}$$

1. K_O is a two-dimensional convolution kernel, considered as a phenomenological scatter propagation kernel. The parameters of K_O are adjusted with a calibration phantom composed of lucite with two cylindrical holes by comparing reconstructions obtained with the beam stops method to those obtained with the API method.

2. The function P is formulated theoretically by integration of the equations which describe first-order Compton interactions of the X-rays beam within the examined object and modelizes both scatter creation and scatter absorption within it. Assuming that $L(x, y)$ is the physical width of the patient crossed by the primary radiation at detector coordinates(x, y), the Compton attenuation, noted $Att_C(x, y)$, is defined as the width of the examined object weighted by Compton linear cross sections:

$$Att_C(x, y) = \int_{x_m=0}^{L(x,y)} \mu_C^f(x_m) dx_m$$

where μ_C^f stands for the linear macroscopic cross section of Compton scattering in the forward direction.

$P(x, y)$ is expressed in terms of the total measurement radiation $\Phi(x, y)$, of $Att_C(x, y)$, and of a geometrical tabulated parameter $\alpha(L(x, y))$:

$$P(x, y) = \Phi(x, y) \times Att_C(x, y) \times \alpha(L(x, y))$$

$\alpha(L(x, y))$ takes into account the fact that the mean path lenght of a scattered photon is greater than the mean patient width. A first reconstruction is performed with raw projection data. Then, a thresholding is performed on the attenuation coefficient data to separate air and soft tissues regions to have an approximation of μ_C^f for each voxel. Determination of μ_C^f is based on the data taken from ICRU Report 44 [8]. The integration is performed numerically to obtain $Att_C(x, y)$.

3. A is a 2D proportionality image which quantifies the ratio between the scattered radiation and the first-order scattered radiation at each detector pixel.

1.3 Transposition coefficients evaluation

The transposition coefficients TC are formulated as the ratio between the model of scatter applied to the examined tomographic projection ϕ_S^{PR} and that applied to the calibrated lucite equivalent scattered radiation map ϕ_S^{CA}:

$$TC = \frac{\phi_S^{PR}}{\phi_S^{CA}}$$

A is assumed to be constant for a given attenuation. Thereby, the quite tedious analytical evaluation of multiple-order Compton scatter has not to be performed assuming that A image is the same for a projection and for the associated lucite equivalent scattered radiation map. Thus:

$$TC(x,y) = \frac{P^{PR}(x,y) * K_O(x,y)}{P^{CA}(x,y) * K_O(x,y)}$$

where $P^{PR}(x,y)$ and $P^{CA}(x,y)$ correspond to the P function for the examined tomographic projection and for the lucite equivalent scattered radiation map respectively.

Knowing that P^{CA} image has low frequencies compared to K_O frequencies, transpositions coefficients are finally estimated by:

$$\boxed{TC(x,y) = \left(\frac{P^{PR}(x,y)}{P^{CA}(x,y)}\right) * K_O(x,y)}$$

The global scheme of the method is illustrated in the figure 1.

2. Experimental results

2.1 Experimental setup

All images are acquired using a conventional X-rays tube (tungsten anode, focus 1.5×1.5 mm, beryllium output window) and a digital flat panel detector (Thales Flashscan 33 HE, a:SI technology, Lanex Fast® scintillator, dimension of the active area : 406 mm $\times$ 285 mm , number of pixels : 3200 $\times$ 2304 , pixel size :127 micrometers,16 bits). The radiological constants are 120 kV, 5 mA, 2.8 s. The source filtering is obtained with 2 mm of copper and 2 mm of steel. The source to detector distance is 2180 mm and the distance between the center of the object and the detector is 330 mm.

A classical method of scatter estimation using beam stops has been adapted to tomographic acquisitions: scatter estimation has been applied to each projection of the tomographic acquisition. During the acquisitions of this study, typically 36 central beam stops have been imaged. Different beam stops positions were imaged for each tomographic projection by translating the beam stops vertically and horizontally. In this way, scatter is better sampled than with a single acquisition with the beam stops.

Calibration objects are lucite plates of dimensions 500 mm $\times$ 500 mm with thicknesses 50, 100, 125, 150, 175, 200, 225, 250 and 275 mm respectively. Due to the limited power of the X ray tube, image averaging was processed on 16 frames to obtain calibration plates acquisitions presenting smaller noise to signal ratio compared to that of on-line acquisitions.

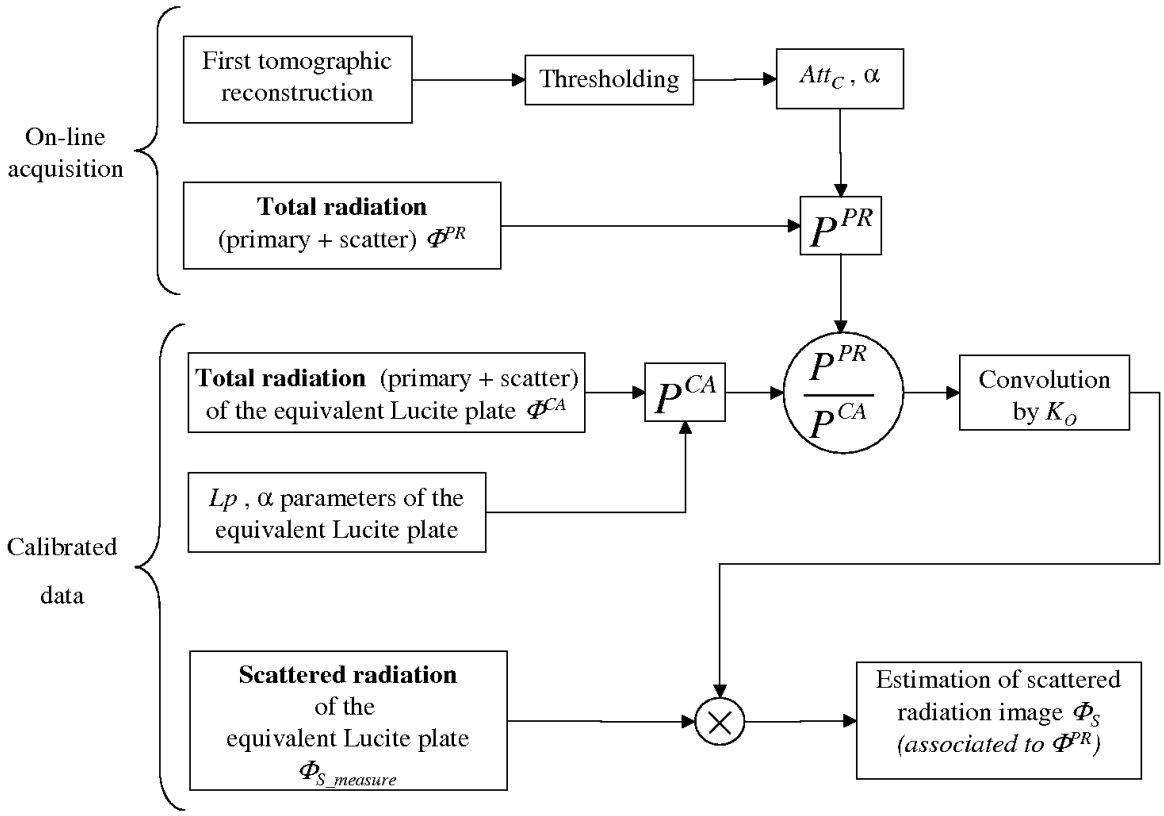

Figure 1: Scheme of the API correction method

2.2 Results on a lucite phantom

720 projections over 360° of a lucite phantom with two cylindrical holes were collected by the X-rays rotational tomographic system without anti scatter grid. Due to the limited size of computer RAM, 4×4 binning was performed on tomographic acquisitions to obtain projections composed of 800×576 pixels images.

The lucite phantom is the phantom used to calibrate the standard deviation of the phenomenological scatter propagation kernel K_O. In the configuration without antiscatter grid, this kernel is approximated by a circularly symmetric Gaussian function. The standard deviation of K_O was adjusted by comparing the reconstructions obtained with the API method to that obtained using the beam stops method.

Eight different beam stops positions were imaged for each tomographic projection to sample scattered radiation images correctly. Thus, the global acquisition time has been multiplied by a factor 9 by comparison with a single acquisition.

Feldkamp algorithm was used to obtain reconstructed images from three experimental acquisition sets: without scatter correction, with correction by classical beam stops method and with correction by the API method. Simulated projections of primary radiation were performed with the simulation software Sindbad, developed at CEA LETI [9]. The data set is reconstructed in $900 \times 700 \times 100$ voxels (voxel size $0.4 \times 0.4 \times 0.4$ mm) by the Feldkamp algorithm.

The figure 2 illustrates the results obtained on reconstructed images of the lucite-air phantom. Horizontal profiles corresponding to cross-hatched lines of reconstructed images are illustrated on the figure 3. Scatter flux in the projections leads to cupping artifact. This phenomenon results in an under-estimation of reconstructed linear attenuation in the central zone of the reconstructed image. The profiles show the cupping artifact when the X-rays scatter is not corrected. This artifact is removed when a correction is applied. A gain of 50% in accuracy for the linear attenuation is performed at the center of the phantom by correcting X-rays scattered radiation.

Quantitative improvements of tomographic reconstructions obtained with the new digital scatter correction method have the same order of magnitude as the beam stop array technique, with an acquisition time reduced by a factor 9.

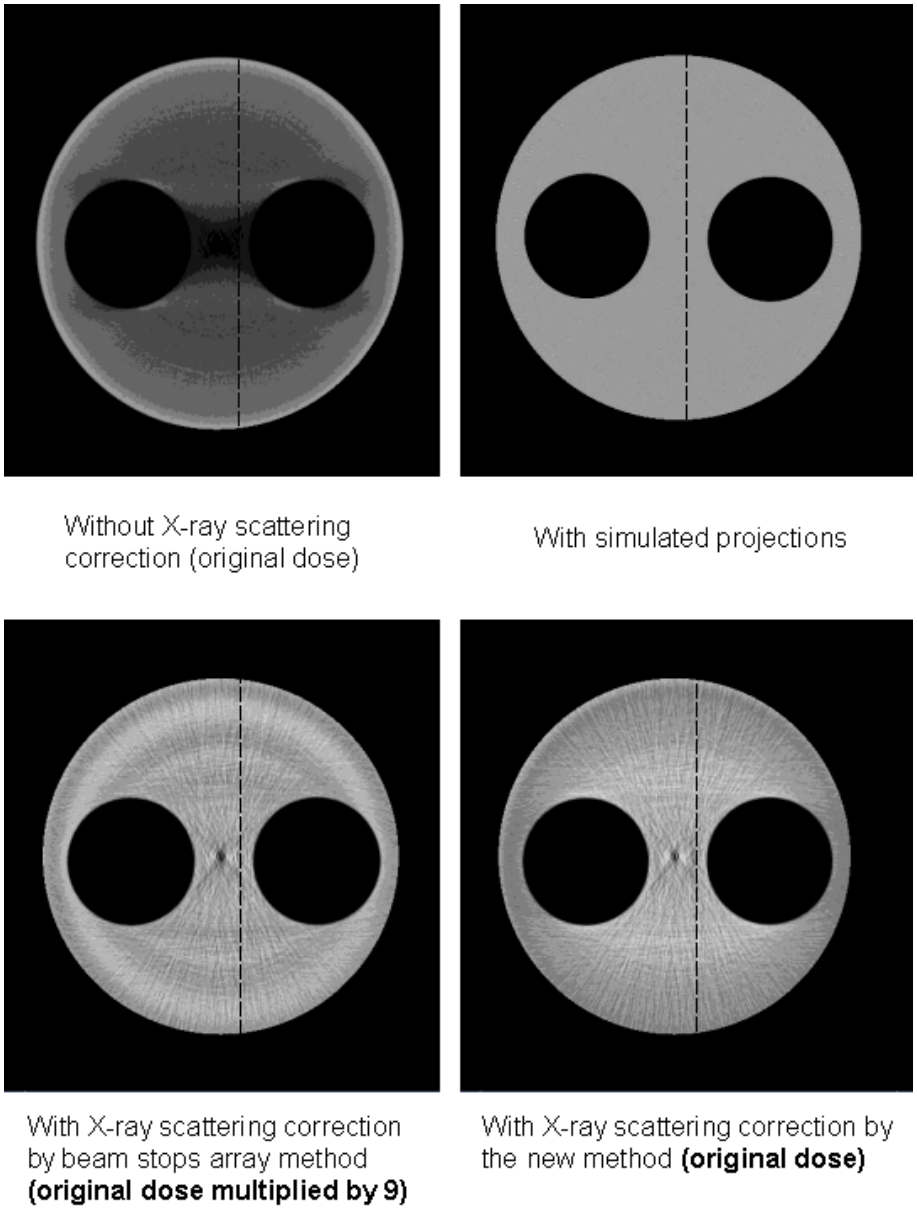

Figure 2: Reconstructed images of the central plane of the lucite-air phantom.

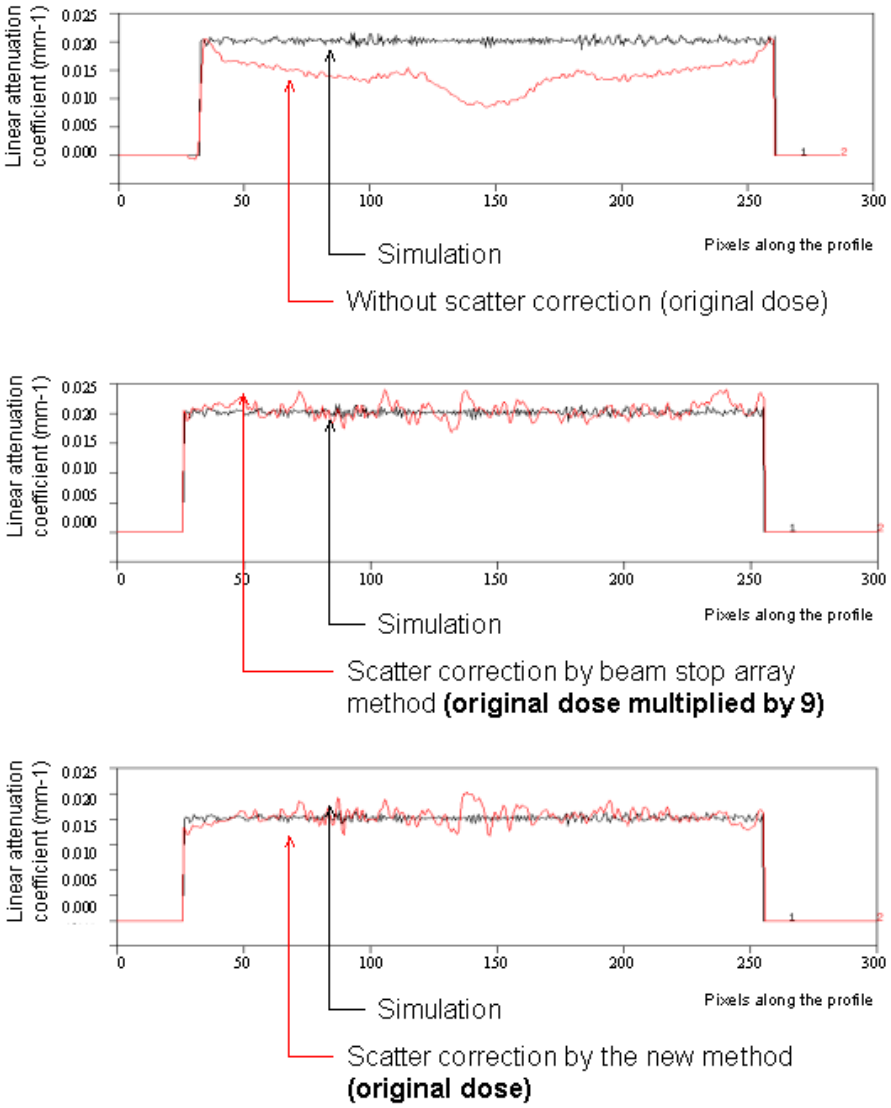

Figure 3: Central profiles of reconstructed central planes of the lucite-air phantom (represented with cross-hatched lines in reconstructed images of figure 2))

2.3 Results on a phantom with metallic inserts

The phantom with metallic inserts is a right circular cylinder made of water. It comprises two hollow cylinders made of lucite and cylindrical metallic inserts made of brass. 360 projections over 180° of the phantom were collected by the X-rays rotational tomographic system with an antiscatter grid (Smit Röntgen®, 36 lines/cm, ratio r=12).

The API method has been adapted to the experimental bench with an antiscatter grid. As scatter propagates preferentially in the direction of the strips of the grid, K_O is approximated by a two-dimensional Gaussian function with two different standard deviations: a high standard deviation in the direction of the strips and a low standard deviation in the direction perpendicular to the strips. The two-dimensional convolution kernel K_O has been adjusted with acquisitions of the lucite-air phantom performed with the antiscatter grid.

Four different beam stops positions were imaged for each tomographic projection to sample scattered radiation images. The figure 4 illustrates a tomographic projection obtained by combining the four beam stops acquisitions. Different profiles corresponding to the horizontal line of the figure 4 are plotted on figure 5. These profiles show that our beam stops method is not able to estimate scatter: scattered radiation images are under-sampled. For example, the estimated scatter is higher than the total radiation on some high frequencies regions. Results of the API method are plotted on the figure 6. The reconstructed image is more contrasted when the scatter correction is applied on tomographic projections.

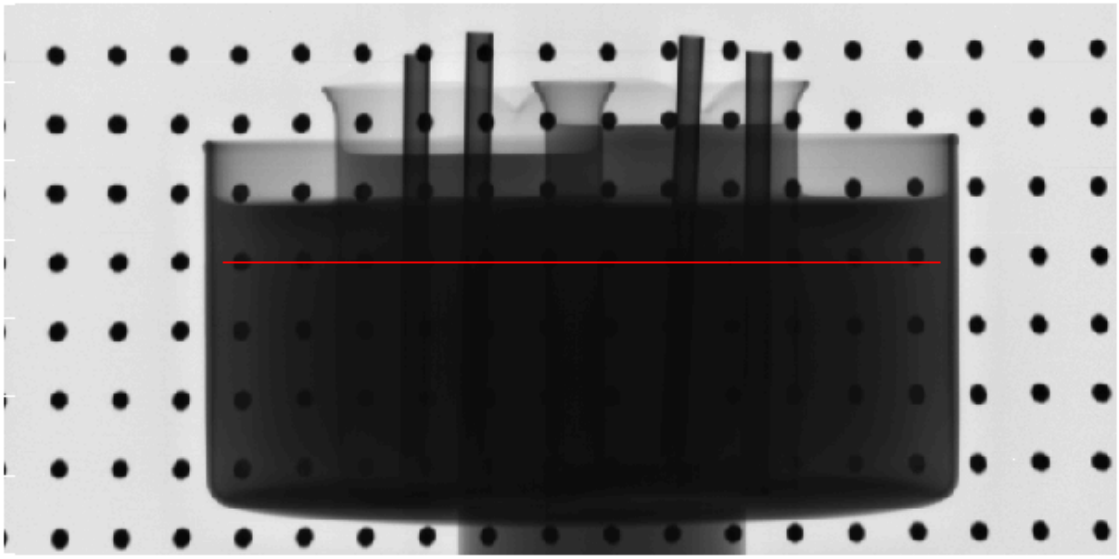

Figure 4: Tomographic projection obtained by combining the four beam stops acquisitions

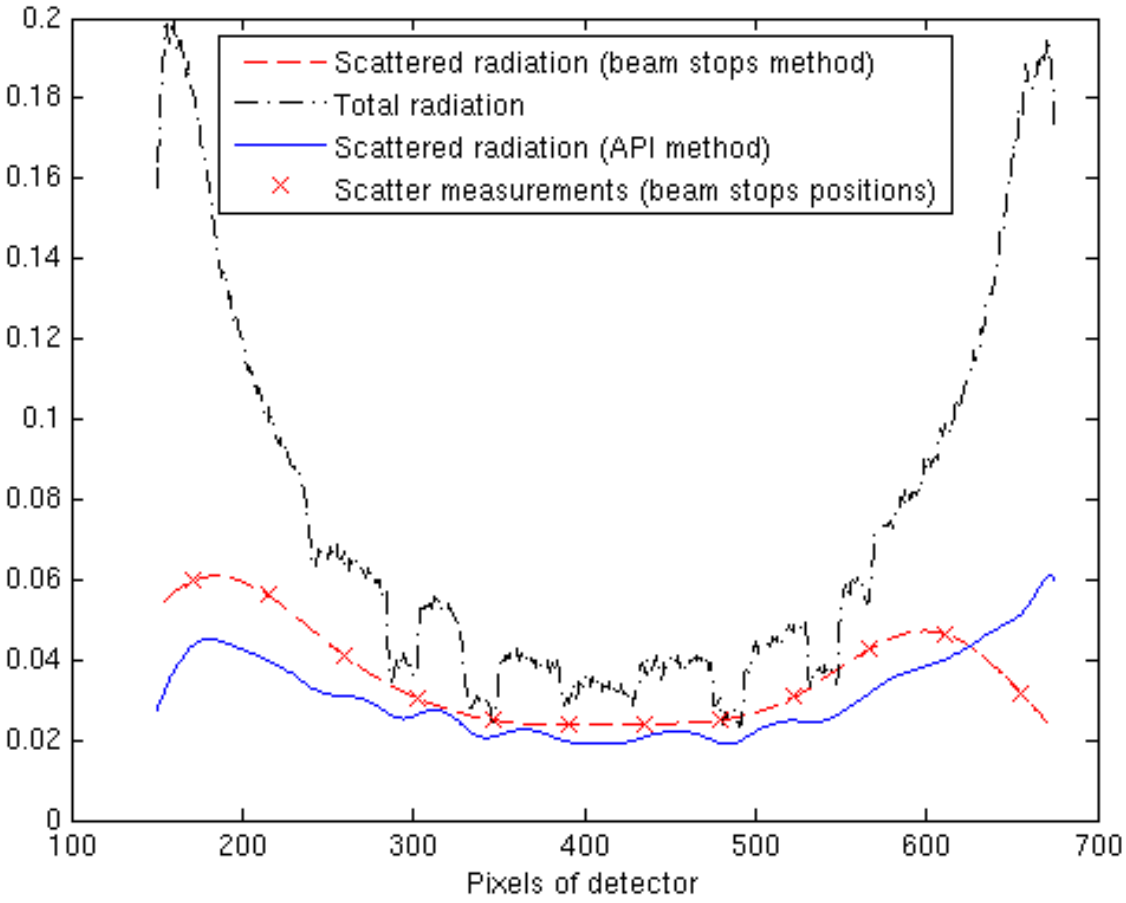

Figure 5: Profils corresponding to the horizontal line of the figure 4.

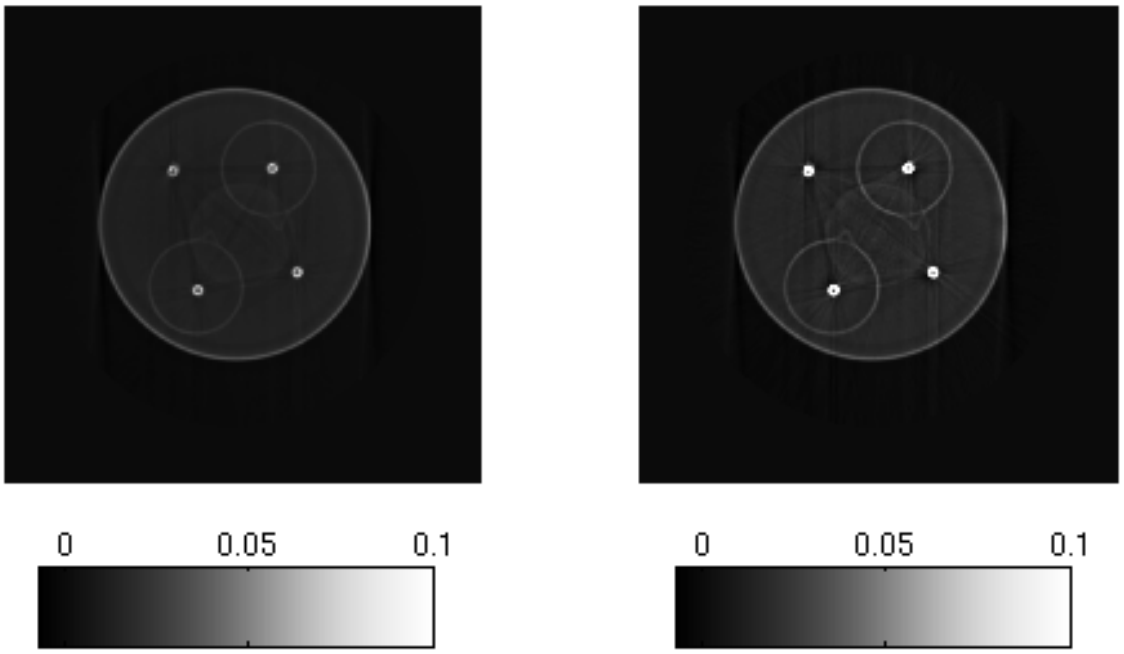

Figure 6: Reconstructions of the water phantom with metallic inserts without scatter correction (left) and with scatter correction by the API approach (right).

3. Discussion

The originality of the method proposed in this work is in coupling the use of three-dimensional data issued from the first reconstruction with projections and calibrated data. The 3D data

are used by numerical integrations of differential Compton scatter cross-sections along path lines of primary radiation. Thereby, the new algorithm of object scattering correction needs significantly lower computation times compared to Monte Carlo based methods.

The performances of the API method have been investigated with and without antiscatter grid. Without antiscatter grid, improvements of tomographic reconstructions obtained with the API method had the same order of magnitude as the beam stop array technique, with an X-rays dose reduced by a factor 9. With the antiscatter grid, reconstructions were performed with tomographic acquisitions of a water phantom with metallic inserts. In this configuration, the beam stops method is not able to sample scatter correctly when four different beam stops acquisitions are combined (the acquisition time is multiplied by 5 compared to a single acquisition). When the scattered radiation is corrected by the API method, the reconstruction is more contrasted compared to that performed without scatter correction.

4. Conclusion

This work gives a response to a fundamental problem of tomographic reconstruction with flat panel 2D detector. Previous studies showed the great efficiency of the API method for X-rays scatter correction for 3D quantitative tomographic reconstructions in medical field [6] [7]. This study demonstrates that it is possible to adapt the API method to CND applications.

Acknowledgments

The authors wish to thank Georges Gonon and Thomas Bordy for valuable assistance in the carrying out of experimental setup.

References

[1] M. Zellerhoff, B. Scholz, E.-P. Rührnschopf, and T. Brunner, "Low contrast 3d-reconstruction from c-arm data," *Proceedings of SPIE Medical Imaging, San Diego* **5745**, 2005.

[2] A. P. C. W. Zbijewski and F. J. Beekman, "Monte carlo based scatter correction for cone-beam micro ct," *Proceedings of The 7th International Conference on Fully 3D Reconstruction In Radiology and Nuclear Medicine. Saint Malo, France. June 29-July 4, 2003* , 2003.

[3] R. Ning, X. Tang, and D. Conover, "X-ray scatter correction algorithm for cone beam CT imaging," *Medical Physics* **31**, pp. 1195–1202, 2004.

[4] M. Endo, T. Tsunoo, N. Nakamori, and K. Yoshida, "Effect of scattered radiation on image noise in cone beam ct," *Medical Physics* **28**, pp. 469–474, 2001.

[5] J. Dinten, M. Darboux, T. Bordy, C. Robert-Coutant, and G. Gonon, "X-rays scatter correction for dual energy x-rays absorptiometry: compensation of patient's lean/fat composition," *Proceedings of SPIE Medical Imaging, San Diego* **5368**, 2004.

[6] J. Rinkel, L. Gerfault, F. Estève, and J. Dinten, "Experimental evaluation of a physical based approach of scattered radiation correction in thoracic cone beam CT," *submitted to Medical Physics* , 2006.

[7] J. Rinkel, L. Gerfault, F. Estève, and J. Dinten, "Evaluation of a physical based approach of scattered radiation correction in cone beam CT with an anthropomorphic thorax phantom," *Proc. SPIE: Medical Imaging Conference* **6142**, 2006.

[8] "Tissue substitutes in radiation dosimetry and measurement," tech. rep., Report 44 of the International Commission on Radiation Units and Measurements (Bethesda, MD), 1989.

[9] A. Glière, "Sindbad: From cad model to synthetic radioagraphs," *Review of progress in QNDE* **17A**, pp. 387–394, 1998.